Characterization of Vanadium and Titanium Oxide Supported SBA-15

Y. Segura,*,† P. Cool,† P. Kustrowski,‡ L. Chmielarz,‡ R. Dziembaj,‡ and E. F. Vansant†

Department of Chemistry, Laboratory of Adsorption and Catalysis, University of Antwerp (UA), Universiteitsplein 1, B-2610 Wilrijk, Belgium, and Faculty of Chemistry, Jagiellonian University, Ingardena 3, 30-060 Krakow, Poland

Received: February 14, 2005; In Final Form: April 13, 2005

Supported vanadium and titanium oxide catalysts were prepared by adsorption and subsequent calcination of the vanadyl and titanyl acetylacetonate complexes, respectively, on mesoporous SBA-15 by the molecular designed dispersion (MDD) method. Liquid and gas phase depositions at different temperatures were carried out with vanadyl acetylacetonate, and the different results together with those of titanyl acetylacetonate in the liquid phase deposition were discussed. The bonding mechanism, the influence of the metal interaction with the support material, and differences due to the way of deposition and the temperature were investigated by TGA, chemical analysis, FTIR, and Raman spectroscopy. Elevated dissolving temperatures in the liquid phase led to higher final loadings on the SBA-15 without the formation of clusters, even at high loadings. The decomposition of the anchored vanadium and titanium complexes, their thermal stability, and the conversion to the covalently bound VO_x and TiO_x species on SBA-15 were studied and investigated by in situ transmission IR spectroscopy. In general, the titanium complex is more reactive than the vanadium complex toward the surface of SBA-15 and has a higher thermal stability. The MDD method of the $VO(acac)_2$ and $TiO(acac)_2$ enables to create a dispersed surface of supported VO_x and TiO_x, respectively. The structure configurations of VO_x and TiO_x oxide catalysts obtained at different metal loadings were studied by Raman spectroscopy. Pore size distributions, XRD, and N_2 sorption confirmed the structural stability of these materials after grafting. VO_x/SBA-15 and TiO_x/SBA-15 samples, with different metal loadings, were also catalytically tested for the selective catalytic reduction (SCR) of NO with ammonia.

1. Introduction

Metal oxide dispersions in mesoporous materials have been of great interest by means of the incorporation of transition metals in the framework of the support material. The first publication related to this domain was the incorporation of Fe_2O_3 particles in MCM-41.[1] Since then, much more work has been done in the field of transition metal oxides supported on different porous materials. One of the most common methods for the preparation of metal oxide dispersions on mesoporous materials is the impregnation with solutions of precursor salts.[2,3] The materials described in this work are no longer prepared by the conventional methods but are the result of a molecular designed dispersion (MDD)[4] method of active elements on carefully prepared micelle templated structures (MTS)[5] using their acetylacetonate complexes.

The interest of using these complexes is the requirement of obtaining a high dispersion of catalytic active sites on support materials. Their bulky acetylacetonate (=acac) ligands are able to isolate the central metal ion on the surface, allowing high dispersions. Following the MDD process, metal acac complexes are reacted with the surface hydroxyls of the support material and converted into the metal oxide form after calcination. Both liquid and gas phase depositions have been performed to deposit metal acac complexes on different supports.[6] A great variety of acac complexes on different supports have already been studied and reported in the literature.[7−10]

Materials containing vanadium and titanium oxides are known as excellent catalysts in several redox reactions. Vanadium oxide is a powerful redox catalyst in many industrial processes, and it is used in oxidation reactions for the manufacturing of important chemicals.[11] Titanium oxide, when it is on a silica support, is mainly used as a photocatalyst, acid catalyst, and redox catalyst. TiO_2 is widely used as well for many oxidation reactions of organic molecules requiring a high disperse layer on the support.[12] Catalysts based on V_2O_5/TiO_2 are mainly used in the reduction of nitrogen oxides. The selective catalytic reduction (SCR) of NO_x with ammonia is important to reduce emissions of NO from waste gases of stationary sources. However, the use of a silica support instead of titania offers advantages because of the higher surface area and higher resistance to sintering. The V_2O_5/TiO_2 system has already been studied widely well.[13,14] In this paper, the systems VO_x/SBA-15 and TiO_x/SBA-15 are fully characterized and studied separately for the SCR reaction.

For the SCR reaction, the vanadia content in the catalyst is preferably lower than the amount required for a monolayer coverage,[15,16] but for other types of oxidation reactions, a higher loading is required with a high dispersion.[17−19] Therefore, the importance of tuning and controlling the final loading of metals and their dispersion on the support material by different deposition methods and temperatures is obvious.

$VO(acac)_2$ and $TiO(acac)_2$ have already been deposited on different supports such as silica,[20] alumina,[21] MCM-48,[22] or zirconia.[23] Recently, the oxidation of bulkier molecules has required the synthesis of a material like SBA-15, which is a

* Corresponding author. E-mail: yolanda.segura@ua.ac.be.
† University of Antwerp (UA).
‡ Jagiellonian University.

10.1021/jp0507750 CCC: $30.25
Published on Web 05/27/2005

mesoporous silica molecular sieve with uniform pores. It is characterized by a very high pore volume, thick pore walls, and intrinsically combined micro- and mesopores with a high surface area.[24]

In this study, we present different methods to prepare TiO_x and VO_x on SBA-15 following the MDD method. A detailed characterization of the catalyst precursors (before calcination) and the final VO_x/SBA-15 and TiO_x/SBA-15 samples (after calcination) is performed using IR transmission spectroscopy following their conversion to the covalently bound VO_x and TiO_x species on the SBA-15 surface. Additional characterization is obtained by FTIR-PAS, TGA, chemical analysis, FT-Raman, and N_2 sorption measurements.

VO_x/SBA-15 and TiO_x/SBA-15 were catalytically tested in the SCR of NO with ammonia. The catalytic performance of the samples depends on the metal loading. VO_x/SBA-15 catalysts are active in a low temperature range; however, an increase of their activity is observed in the high temperature range, while the TiO_x/SBA-15 catalysts are not active below 250 °C.

2. Experimental Section

2.1. Sample Preparation and Treatment. *2.1.1. Support.* SBA-15 was prepared by using 4 g of Pluronic P123 triblock copolymer surfactant ($EO_{20}-PO_{70}-EO_{20}$) dissolved in a 2 M water/HCl solution. Subsequently, an amount of tetraethyl orthosilicate (TEOS) was added. The resulting mixture was stirred for 8 h at 45 °C and then aged for 15 h at 80 °C. The white product was filtered, washed, and dried. The sample was subsequently calcined at 550 °C at 1 °C/min for 6 h in air atmosphere.

2.1.2. Metal Deposition. Single depositions of the vanadium and titanium metal oxides on the ordered mesoporous material SBA-15 were done by the MDD method of their acetylacetonate complexes. The $TiO(acac)_2$ and $VO(acac)_2$ complexes both have the same structure, except for the fact that $TiO(acac)_2$ is present as a bidentate complex ($[TiO(acac)_2]_2$), which consists of a cyclic dimer with the Ti atoms linked through oxygen atoms.

Liquid phase deposition was performed by the deposition of the metal acetylacetonate complex ($VO(acac)_2$ or $TiO(acac)_2$) onto the SBA-15 surface by the designed dispersion method using toluene as a solvent. An amount of $TiO(acac)_2$ or $VO(acac)_2$ was dissolved in 100 mL of zeolite dried toluene. The dried SBA-15 was then added, and the solution was stirred for 1 h. After reaction, the modified support was filtered off, washed a few times with toluene, and dried under vacuum. The reaction was carried out at RT and in the absence of air. Liquid phase deposition was also carried out by dissolving the acetylacetonate complex at 45 °C. After adding the SBA-15 support at 45 °C, the temperature was dropped to room temperature in an hour while the suspension was stirred. After reaction, the modified support was filtered off, washed a few times with toluene, and dried under vacuum.

SBA-15 supported vanadium oxides were also obtained by a gas phase deposition avoiding the use of the organic solvents. The gas phase modification of the SBA-15 with $VO(acac)_2$ was carried out by placing both components in a glass holder initially under vacuum at RT. The temperature was increased, and the sublimed vanadium complex reacted with the surface of SBA-15. The excess of $VO(acac)_2$ was removed, by taking out the modifier holder inside of the glass holder. Gas phase deposition using the $TiO(acac)_2$ complex was not possible. It was found in previous research that a very small amount of titanium and acac ligands were detected after a reaction at high temperature, because of decomposition of the complex (not sublimation).[22] The SBA-15 materials with adsorbed complexes, obtained from the liquid and gas phases were called the precursors. The acac ligands were removed by calcination, which was performed in a programmable oven at 550 °C in ambient air, resulting in a final vanadium or titanium oxide catalyst.

2.2. Characterization Methods. The concentration of the metals on the support was determined by UV−vis spectrophotometry after destruction of the samples and measured colorimetrically. The measurements were performed on a Unicam 8700 UV−vis instrument. The samples were stirred for 20 min in hot sulfuric acid (2.5 M). After filtration, H_2O_2 was added, and the vanadium and titanium concentrations were measured at 450 and 407 nm, respectively.[25]

Photoacoustic infrared spectra (FTIR-PAS) were recorded on a Nicolet 20 SX spectrometer, equipped with a McClelland photoacoustic cell, to ensure IR measurements under dry conditions. About 1000 scans were taken with a resolution of 8 cm^{-1}. The PAS spectrometer was placed in an isolated bench, which was constantly purged with dry nitrogen to ensure complete dry conditions.

Transmission spectra were measured on a Nicolet20SX spectrometer equipped with a vacuum system cell and a DTGS detector and using a home-built in situ vacuum IR transmission cell. Self-supporting disks with a thickness of 20 mg/cm^2 were used. One hundred scans were measured with a spectral resolution of 4 cm^{-1}.

FT-Raman spectra were recorded on a Nicolet Nexus FT-Raman spectrometer with a Ge detector. All samples were measured at room temperature in a 180° reflective sampling configuration, with a 1064 nm Nd:YAG excitation laser. For each spectrum, 2.000 scans were averaged and the laser power was set between 1 and 2 W.

Thermogravimetric (TG) measurements were performed on a Mettler TG50 thermobalance, equipped with a M3 microbalance and connected to a TC10A processor. Samples were heated from 30 to 50 °C and from 50 to 550 °C at a rate of 5 °C/min.

XRD diffractograms were taken on a Philips PW1840 powder diffractometer using Ni-filtered Cu Kα radiation (λ = 1.542 Å)

Porosity and surface area studies were performed on a Quantachrome Autosorb 1 MP instrument. N_2 adsorption/desorption isotherms were recorded at −196 °C. The Brunauer−Emmett−Teller (BET) model was used to calculate the specific surface area. Micropore volume was calculated by the t-plot analysis, and the total pore volume was calculated by means of the total amount of adsorbed gas at $P/P_0 = 0.98$. The samples were outgassed overnight at room temperature for the precursors or at 200 °C for the supported oxides.

The catalytic experiments were performed at atmospheric pressure in a fixed-bed flow reactor (inside diameter, 7.0 mm; length, 240 mm). The reactant concentrations were continuously measured using a quadrupole mass spectrometer (VG QUARTZ) connected to the reactor via a heated line. Prior to the reaction, each sample of the catalyst was outgassed in pure helium at 200 °C for 30 min. Samples of 100 mg of the catalyst were used. At the reactor inlet, the composition of the gas mixture was $[NO] = [NH_3] = 2500$ ppm, $[O_2] = 2.5\%$, and He as a balancing gas at a total flow rate of 40 mL/min. The reaction was studied at temperatures ranging from 100 to 550 °C. The intensities of the mass lines corresponding to all reactants and products were measured at a given temperature for 15−30 min

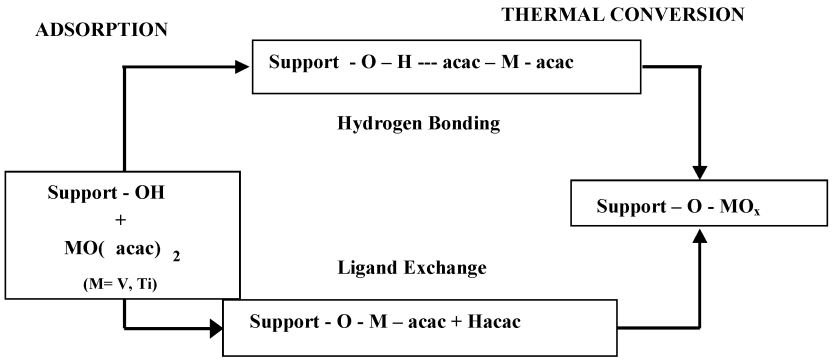

Figure 1. Schematic representation of the "molecular designed dispersion" method of acetylacetonates.

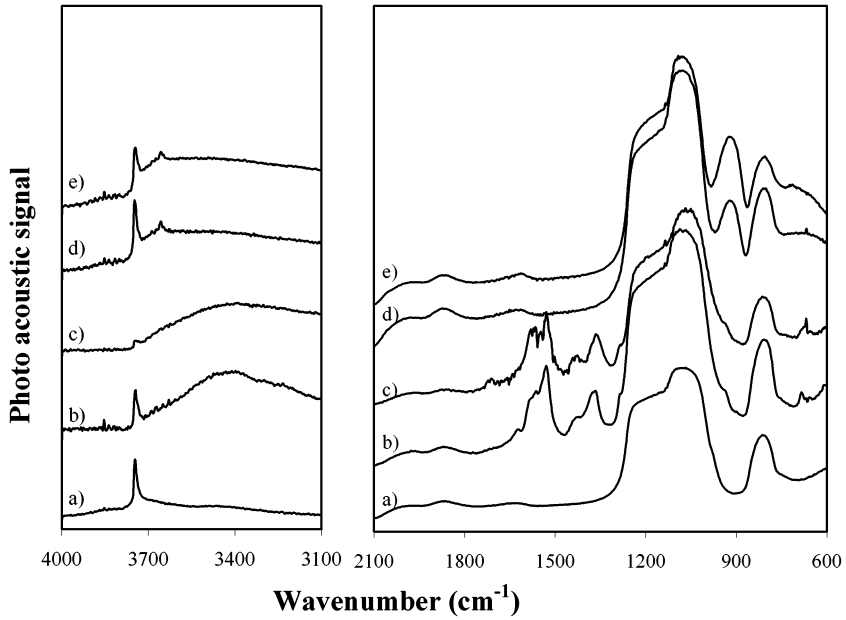

Figure 2. FT-IR spectra of (a) pure SBA-15 and SBA-15 supported vanadium oxides: (b) precursor deposited by the liquid phase method; (c) precursor deposited by the gas phase method (at 140 °C); (d) liquid phase deposition calcined sample; (e) gas phase deposition calcined sample.

after the reaction reached a steady state. The signal of the helium line served as the internal standard to compensate for small fluctuations of the operating pressure. The sensitivity factors of the analyzed lines were calibrated using commercial mixtures of gases. The possible changes in the molar flow caused by the NO and NH_3 conversion were negligible in the diluted reaction mixtures. The conversion (expressed in percent) was calculated by the difference between inlet and outlet molar flow of the reactants in the reactor.

3. Results and Characterization

3.1. Characterization of the Precursors. The $TiO(acac)_2$ and $VO(acac)_2$ acetylacetonate complexes were grafted on the surface of the SBA-15 following the MDD method. A schematic representation of this MDD mechanism is depicted in Figure 1.

The adsorption of the complexes on the support follows two different mechanisms. One is by hydrogen bonding between an acetylacetonate ligand and the surface hydroxyls, and the other one is by a ligand exchange mechanism in which a covalent metal−oxygen support bond is formed while an acetylacetonate ligand (Hacac) is lost.

The calculation of *R* value allows us to elucidate the reaction mechanism, since it reproduces the number of acac ligands associated with one metal (vanadium or titanium) atom. [26]

$$R = \frac{\text{mmol}_{(\text{acac})}/\text{g}_{\text{total}}}{\text{mmol}_{(\text{TiorV})}/\text{g}_{\text{total}}}$$

A ligand exchange results in an *R* value of 1, because only one acetylacetonate ligand remains bonded to the metal atom. For the hydrogen bonding, an *R* value of 2 can be obtained, since there is no loss of any of the acac ligands.[20,22]

3.1.1. $VO(acac)_2$/SBA-15 Support. According to this MDD method, the surface of SBA-15 was modified with different amounts of V, using vanadyl acetylacetonate as the V source, under liquid phase and gas phase conditions and at different temperatures.

In Figure 2, the infrared spectra are shown for the pure SBA-15 and the SBA-15 supported vanadium oxide precursors and final VO_x catalyst obtained by gas phase and liquid phase deposition.

The same initial concentration (0.75 g of $VO(acac)_2$) was used by liquid and gas phase deposition of the vanadium complex. However, a higher vanadium loading was obtained by the gas phase deposition at 180 °C (1.5 mmol/g) compared to the loading obtained on the surface of SBA-15 by the liquid phase deposition at RT (0.4 mmol/g).

TABLE 1: Structural Properties, Vanadium Loadings, and *R* Values of Blanks, Precursors, and Final Vanadium Oxide Catalysts on the SBA-15 Support

sample	S_{BET} (m^2/g) (loss %)	micropore vol (cc/g)	total pore vol (cc/g)	V loading (mmol/g)	V atoms/nm^2	*R* value
			Liquid Phase (RT)			
SBA-15 blank	735	0.146	0.76			
SBA-15/VO(acac)$_2$ prec.	319	0.001	0.46			
SBA-15/VO_x	557 (24%)	0.094	0.62	0.4	0.33	2.0
			Gas Phase (140 °C)			
SBA-15 blank	735	0.146	0.76			
SBA-15/VO(acac)$_2$ prec.	171	0.004	0.24			
SBA-15/VO_x	463 (37%)	0.048	0.56	1.3	1.06	1.2
			Gas Phase (180 °C)			
SBA-15 blank	886	0.150	0.91			
SBA-15/VO(acac)$_2$ prec.	215	0.000	0.28			
SBA-15/VO_x	376 (58%)	0.022	0.48	1.5	1.20	1.0

TABLE 2: Structural Properties and Metal Loadings on SBA-15 Obtained under Liquid Phase Conditions at RT and at 45 °C (Initial Concentration 1 g of acac Complex per 1 g of SBA-15)

sample	S_{BET} (m^2/g) (loss %)	micropore vol (cc/g)	total pore vol (cc/g)	metal loading (mmol/g)	metal atoms/nm^2	*R* value
SBA-15 blank	722	0.125	0.80			
SBA-15/VO_x (liquid phase, RT)	623 (14%)	0.091	0.71	0.45	0.37	2.0
SBA-15 blank	848	0.162	0.99			
SBA-15/VO_x (liquid phase, 45 °C)	630 (26%)	0.078	0.81	0.76	0.54	1.8
SBA-15 blank	717	0.135	0.79			
SBA-15/VO_x (gas phase, 180 °C)	392 (45%)	0.027	0.57	1.65	1.40	1.1
SBA-15 blank	848	0.162	0.99			
SBA-15/TiO_x (liquid phase, RT)	628 (26%)	0.083	0.80	0.92	0.65	1.9
SBA-15 blank	759	0.116	0.88			
SBA-15/TiO_x (liquid phase, 45 °C)	612 (20%)	0.083	0.72	1.10	0.90	1.8

It is shown in Figure 2c that the concentration of vanadium deposited on the surface by gas phase reaction was enough to cover most of the free hydroxyl groups of the silica surface. The silanol band at 3675 cm^{-1} has almost completely disappeared, while in the case of liquid phase deposition (Figure 2b) a noticeable silanol band is still visible although less intense compared to the pure SBA-15 support.

The intensity of the silanol band at 3745 cm^{-1} decreases by increasing the V loading. At the same time, the band at ~930 cm^{-1} assigned to Si−O−V appears and increases as the silanol band decreases in intensity. This band roughly indicates the content of V on the SBA-15 and shifts toward a higher wavenumber with an increase of the V concentration. This can be observed in spectrum d in Figure 2 for a sample deposited under liquid phase conditions where Si−O−V appears at 922 cm^{-1}. The same band appears at 936 cm^{-1}, as is shown in spectrum e of Figure 2 for a sample deposited by gas phase deposition containing a higher V loading. The bands between 1200 and 1700 cm^{-1} are assigned to acac ligands[26] and disappear after thermal conversion toward VO_x. The free silanol band at 3745 cm^{-1} is restored again after calcination, and one new band at 3660 cm^{-1} appears which is attributed to the presence of V−OH surface species.[27] A broad contribution between 3600 and 3400 cm^{-1} assigned to hydrogen bonding interaction is also present. This band appears due to the interaction between vicinal OH groups, as Si−OH and V−OH groups are present.

The structural parameters specific surface area, S_{BET}, mesopore and micropore volume, final V loading, and *R* value for the different types of synthesized samples are summarized in Table 1. Higher loadings can be achieved by a deposition of vanadium under gas phase conditions. This is in accordance with previous studies using other types of supports, such as silica or MCM-48.[4]

Adsorption of the vanadium complex by the gas phase deposition process follows almost exclusively the ligand exchange mechanism, while in the liquid phase the complex interacts with the SBA-15 surface by hydrogen bonding (the *R* value is 2). This is in accordance with the IR spectrum (Figure 2b), which shows a significant absorption in the region between 3600 and 3200 cm^{-1} attributed to the presence of hydrogen bonded silanols.

R values around 1 are obtained for the samples prepared under gas phase conditions by a ligand exchange mechanism. In fact, the broad band at 3600−3200 cm^{-1} is less pronounced in spectrum c of Figure 2. As the treatment temperature decreases (from 180 to 140 °C), the reaction mechanism shows a combination of the two mechanisms (from $R = 1$ to $R = 1,2$).

Experiments reveal that gas phase deposition at higher reaction temperatures leads to an increase in V loading in the final catalyst. As a consequence, the porosity of the calcined sample is slightly reduced as a function of the vanadium loading, as shown in Table 1.

For the deposited sample at 140 and 180 °C, a loss of 37 and 58% in S_{BET}, respectively, can be observed. These decreases in surface area (expressed in percent) are in agreement with the differences in V content (1.3 and 1.5 mmol, respectively). In the case of the gas phase deposition of V, the surface area and mesopore volume are restored to some extent after calcination, but the micropore volume barely increases after removing the organic ligands by a thermal treatment. This can be explained by the high concentration of vanadium deposited on the surface of SBA-15 and a possible migration of the V toward the micropore walls during the calcination process, especially for the 180 °C reaction (Table 1).

Parts A and B of Figure 3 show the N_2 adsorption/desorption isotherms at −196 °C for the blank SBA-15 and samples obtained under liquid and gas phase conditions, respectively. All adsorption/desorption isotherms are type IV according to IUPAC classification and exhibit an H1 hysteresis loop, which is typical for mesoporous materials.[28]

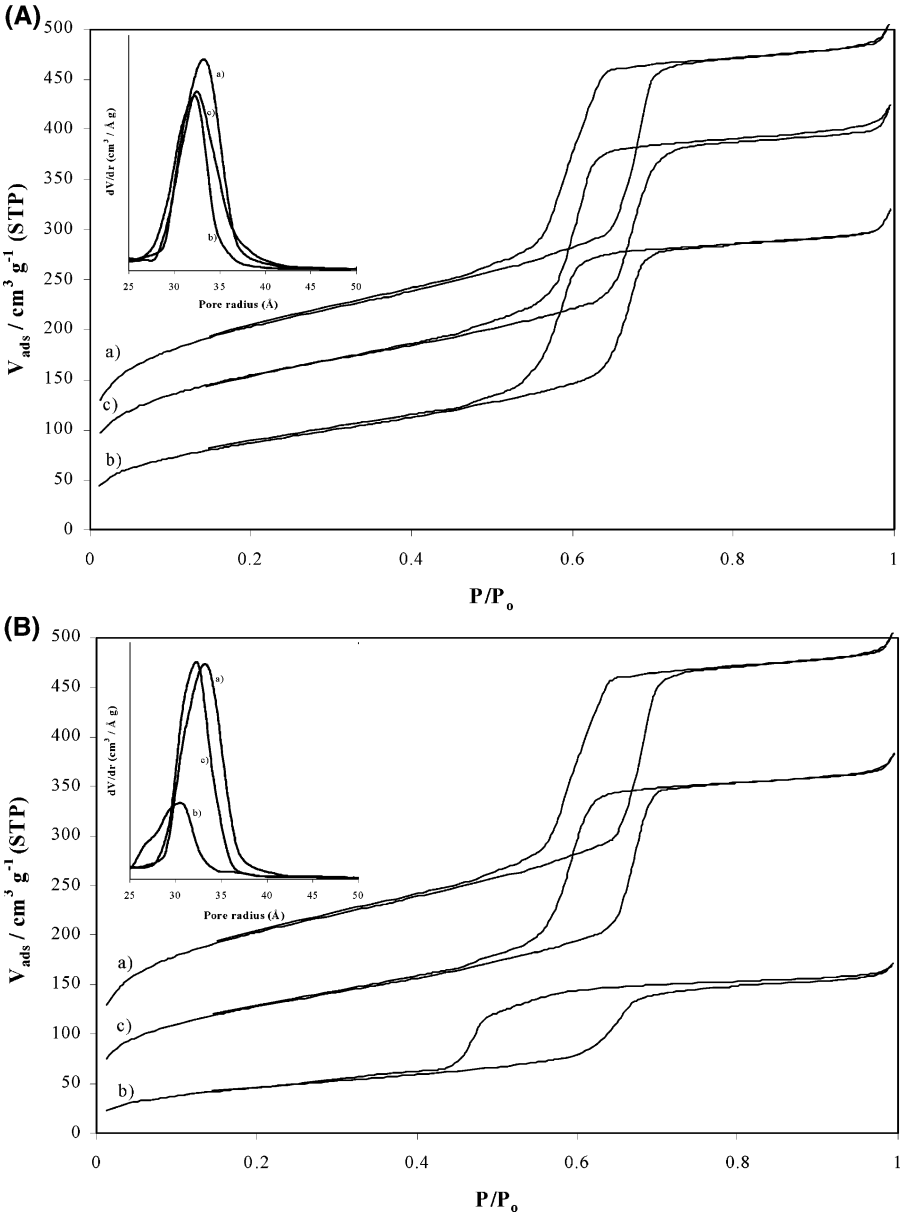

Figure 3. (A) N_2 adsorption/desorption isotherms at −196 °C of SBA-15 supported vanadium oxide samples: (a) pure SBA-15 support; (b) precursor synthesized by the liquid phase; (c) calcined sample synthesized by the liquid phase. The inset shows the corresponding pore size distributions. (B) N_2 adsorption/desorption isotherms at −196 °C of SBA-15 supported vanadium oxide samples: (a) pure SBA-15 support; (b) precursor synthesized by the gas phase; (c) calcined sample synthesized by the gas phase. The inset shows the corresponding pore size distributions .

The isotherms of the calcined SBA-15 and their grafted derivatives exhibit a sharp increase in the adsorbed N_2 volume at $P/P_0 \sim 0.65$, characteristic for capillary condensation within the uniform mesopores of the materials.

The isotherm of the precursor obtained under gas phase conditions containing a high concentration of vanadium is shown in Figure 3B-b. The precursor shows an ink-bottle type of hysteresis, which indicates the presence of pores that are very narrow at the entrances. This will be the result of the dimensions of the metal complexes inside the channels of SBA-15. The precursor obtained under liquid phase conditions (Figure 3A-b) does not show this type of hysteresis. Indeed, the concentration of vanadium is lower so that the steric hindrances are limited. After calcination, both deposition conditions show the same type of isotherm (Figure 3A-c and B-c).

The insets of Figure 3 show a typical BJH pore size distribution for SBA-15, V-acac/SBA-15, and VO_x/SBA-15 prepared by liquid phase deposition (Figure 3A) and gas phase deposition (Figure 3B). Pore size distributions of precursor samples (inset Figure 3A-b and B-b) shift to lower values (especially the sample with a high V content deposited under gas phase conditions, Figure 3B-b). After the thermal conversion of the adsorbed complex, the porosity features are restored to a certain extent, due to the removal of the acetylacetonate ligands. The sharp pore size distributions of blank SBA-15 and calcined VO_x/SBA-15 indicate very uniform pores. No peak broadening can be observed, indicating that the deposited layer is highly homogeneous, as will be also confirmed by the absence of bands assigned to cluster VO_x in Raman spectroscopy.

3.1.2. Comparison between $TiO(acac)_2$/SBA-15 and $VO(acac)_2$/SBA-15. TiO_x/SBA-15 catalysts were also prepared by the molecular designed dispersion (MDD) method using a titanyl acetylacetonate complex. They were obtained under the same liquid phase conditions as those for VO_x/SBA-15 samples, followed by a calcination process.

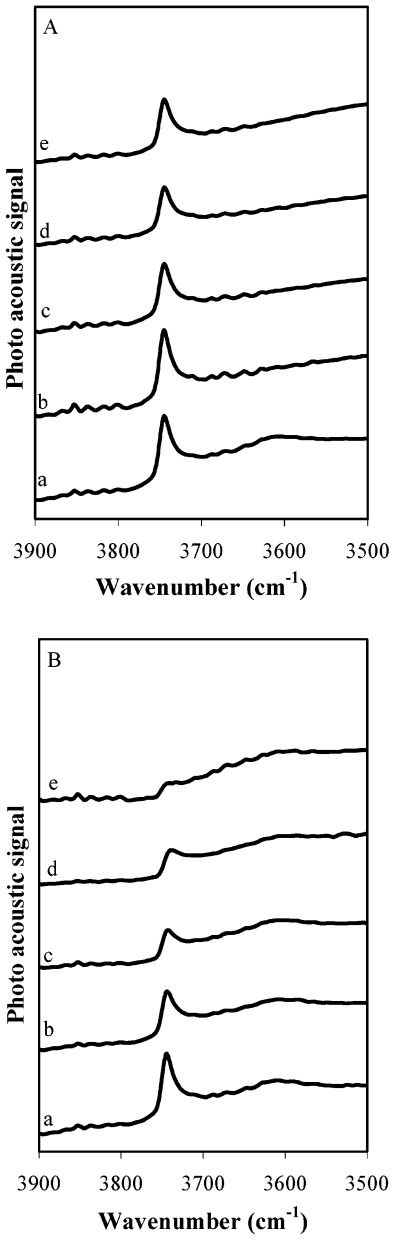

Figure 4. (A) FTIR photoacoustic spectra of VO_x/SBA-15 precursors with a final concentration of (a) 0.17, (b) 0.25, (c) 0.29, (d) 0.36, and (e) 0.43 mmol of V/g. (B) FTIR photoacoustic spectra of TiO_x/SBA-15 precursors with a final concentration of (a) 0.27, (b) 0.45, (c) 0.60, (d) 0.76, and (e) 0.8 mmol of Ti/g.

Parts A and B of Figure 4 show the IR-PAS spectra (range 3500−3900 cm^{-1}) for the precursors of the $VO(acac)_2$ and $TiO(acac)_2$ on the SBA-15 support, respectively. The IR-PAS spectra are given as a function of the final metal loading on the SBA-15 support. The initial concentrations of both metal complexes are the same ((a) 0.1, (b) 0.2, (c) 0.3, (d) 0.5, and (e) 0.8 g of acac complex).

Figure 4B-e evidences almost completely the disappearance of the free silanol band, which means that the Ti complexes are attached to most of the OH on the SBA-15 surface at this concentration (final concentration 0.8 mmol of Ti/g). However, with the same initial concentration, Figure 4A-e shows a clear band of the free silanols, indicating that not all of the surface OH groups have reacted with the V complexes (final concentration 0.43 mmol of V/g).

Figure 5 shows the relation between the different initial concentrations of $TiO(acac)_2$ and $VO(acac)_2$ complexes and the final loading on the SBA-15 surface. Increasing the initial concentration of Ti and V, the final loading also increases until a maximum coverage is reached. From the loadings and the IR data, it is obvious that the titanium complex is more reactive toward the surface of the SBA-15 compared to the $VO(acac)_2$. Although Ti is more reactive than V, the adsorption of their complexes in both cases is mainly controlled by hydrogen bonding with the surface hydroxyl groups, since for all samples *R* values around 2 are found.

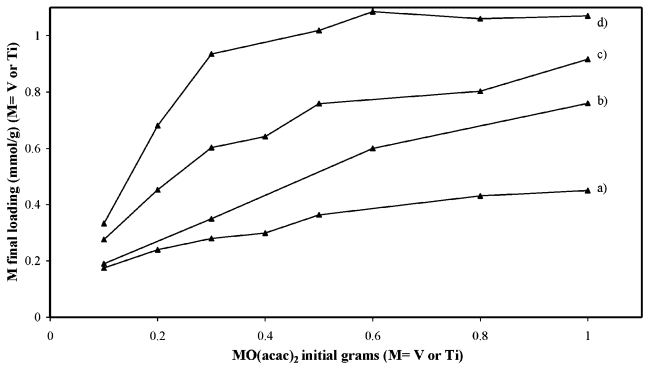

Figure 5. Relation between the initial concentration and the final loading on SBA-15 for $VO(acac)_2$ (a) at RT and (b) at a 45 °C gradient and for $TiO(acac)_2$ (c) at RT and (d) at a 45 °C gradient as a function of final loading (mmol of metal/g) deposited on SBA-15.

To equal the final loading of both metals on the SBA-15 surface under liquid phase conditions, a few parameters were investigated in this work in order to increase the final loading of vanadium on the SBA-15 surface. Experiments show that the amount of solvent used for the liquid phase deposition does not affect the final loading of the metal but that the temperature plays an important role. In fact, when dissolving at high temperature (45 °C), the final loading of VO_x on the SBA-15 is higher than that at RT (Figure 5b). During the reaction, the dissolving temperature is 45 °C and it is followed by a decreasing temperature gradient, the vanadium and titanium loadings on the support are higher compared to RT. This effect is caused by an increase of the solubility of the complexes at higher temperature. Then, during the subsequent decreasing temperature gradient, the solubility of the complex becomes smaller and the excess of complex in the solution is forced to react with the support surface.[29]

The decomposition of the anchored complexes on the SBA-15 support and the conversion of the physisorbed species toward covalently bond VO_x and TiO_x surface groups were studied by using a home-built in situ vacuum IR transmission cell.[30] Transmission IR seems to be the only appropriate spectroscopic technique to follow the calcination process in situ, which is required to understand the reaction mechanism.

The detailed in situ transmission IR study of the single decomposition behavior of the $TiO(acac)_2$ and $VO(acac)_2$ complexes on the SBA-15 surface under liquid phase conditions at RT is presented in parts A and B of Figure 6, respectively.

The interesting region to evaluate is located between 1600 and 1400 cm^{-1}. $TiO(acac)_2$ has a minor absorption at 1440 cm^{-1} and stronger bands at 1580 and 1530 cm^{-1}, whereas $VO(acac)_2$ shows absorptions bands at 1660, 1560, and 1530 cm^{-1} (Figure 6A and B). These bands assigned to V-acac disappear at 200 °C. However, the $TiO(acac)_2$ spectra show the bands of acetylacetonate decrease in intensity only at 300 °C. From these data, it can be concluded that $TiO(acac)_2$ has a higher thermal stability compared to $VO(acac)_2$.

3.2. Characterization of TiO_x and VO_x Oxides Supported on SBA-15 Catalysts. Calcination of the precursor at 550 °C

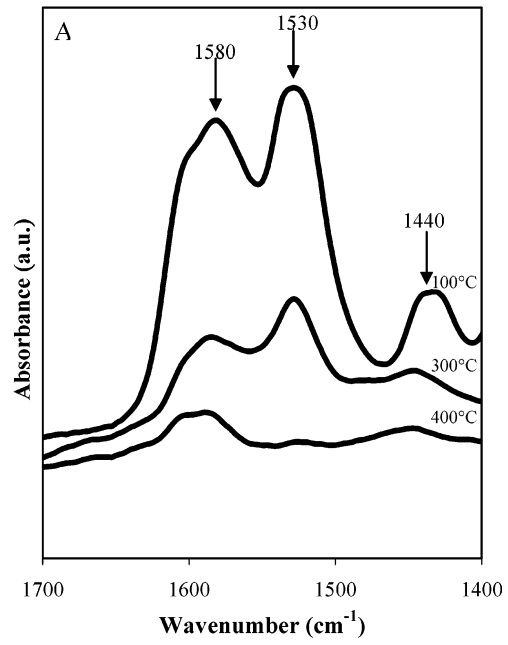

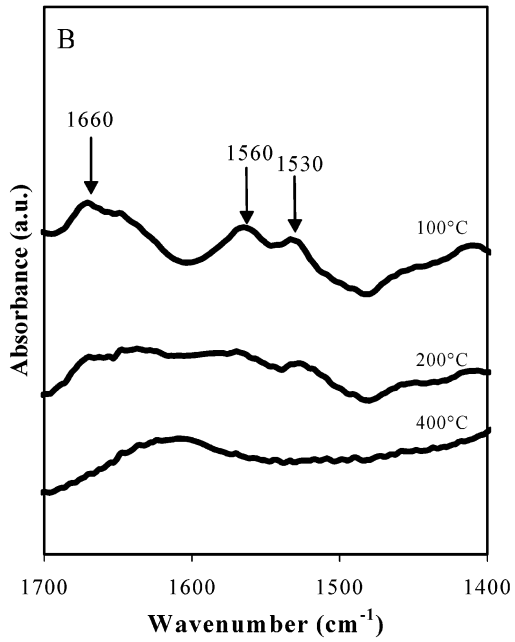

Figure 6. IR spectra of the thermal conversion process of single deposition $TiO(acac)_2$ (A) and $VO(acac)_2$ (B) on SBA-15 as a function of temperature.

in ambient air removes the ligands and yields the final TiO_x and VO_x supported oxide catalysts. In the infrared spectra, all the acac vibration modes disappear, while the band of free silanols of the SBA-15 is partly restored. As shown in Figure 2d,e, the band at around 930 cm^{-1} is assigned to Si−O−V stretch and represents the amount of V on the surface. Furthermore, a band at 965 cm^{-1} can be attributed to Si−O−Ti.

Raman spectroscopy is very sensitive to the presence of TiO_2 and V_2O_5 crystals. TiO_x supported SBA-15 materials obtained by the MDD method do not show typical bands of anatase TiO_2 clusters (638, 519, 399, and 147 cm^{-1}), not even at high concentrations (1.07 mmol of Ti/g) (Figure 7a). The Raman spectra of the samples obtained under liquid phase conditions at 45 °C and under gas phase conditions at 140 °C for the VO_x/SBA-15 (Figure 7b and c) show a clear band at 1042 cm^{-1},

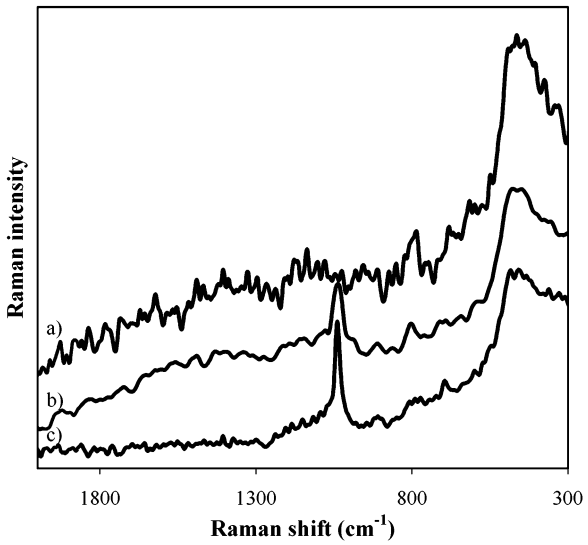

Figure 7. FT-Raman spectra of (a) TiO_x/SBA-15 catalyst prepared by liquid phase deposition (1.07 mmol of Ti/g), (b) VO_x/SBA-15 catalyst prepared by liquid phase deposition (0.76 mmol of V/g), and (c) deposited by the gas phase at 140 °C (1.3 mmol of V/g).

representing isolated vanadia centers in a tetrahedral coordination. Even for the highest V-concentration samples (0.76 mmol of V/g for the liquid phase (Figure 7b) and 1.3 mmol of V/g for the gas phase (Figure 7c)), the bands of VO_x clusters (994, 697, 286, and 147 cm^{-1}) cannot be detected. Therefore, high concentrations of TiO_x and VO_x are obtained on the SBA-15 in the form of isolated titania and vanadia centers in a well-dispersed way.

To study the structural changes of the SBA-15 after grafting with the acac complexes, XRD patterns and N_2 adsorption isotherms at −196 °C were recorded. The XRD diffractograms of blank SBA-15 and the SBA-15 after adsorption of acetylacetonate complexes and its subsequent calcination exhibit one strong reflection (100) at $2\theta \sim 1$ and two weaker peaks (110) and (200) at higher 2θ, associated with hexagonal symmetry and likewise characteristic of the hexagonally ordered structure of SBA-15. Very similar diffraction peaks are observed for the pure and final loaded SBA-15 materials. Therefore, the crystallinity and the ordering of the SBA-15 are retained after the modification of the surface, for both metal oxide samples.

The estimated structural parameters such as specific surface area, S_{BET}, and mesopore and micropore volume after the deposition of the two metal complexes on the SBA-15 surface are summarized in Table 2. The initial concentration for all samples in Table 2 is 1 g of acetylacetonate complex per 1 g of SBA-15. After grafting the surface OH groups with the metal acac complexes, the pores are filled. Therefore, the porosity and surface area are reduced, which increased again after calcination of the precursor as the metal complexes are converted into the vanadium and titanium oxides. The surface area and pore volumes shift to lower values as a function of the metal loading. This reduction of porosity in comparison to the blank support is due to the narrowing of the pores after deposition of the V and Ti acac complexes. However, XRD and S_{BET} characterizations reveal that the deposition of the V and Ti acac complexes and their subsequent thermal conversion results in a supported metal oxide catalyst with the same structure and textural properties as the original SBA-15 material.

3.3. Catalytic Tests in the Selective Catalytic Reduction of NO with Ammonia. The catalytic results obtained for the

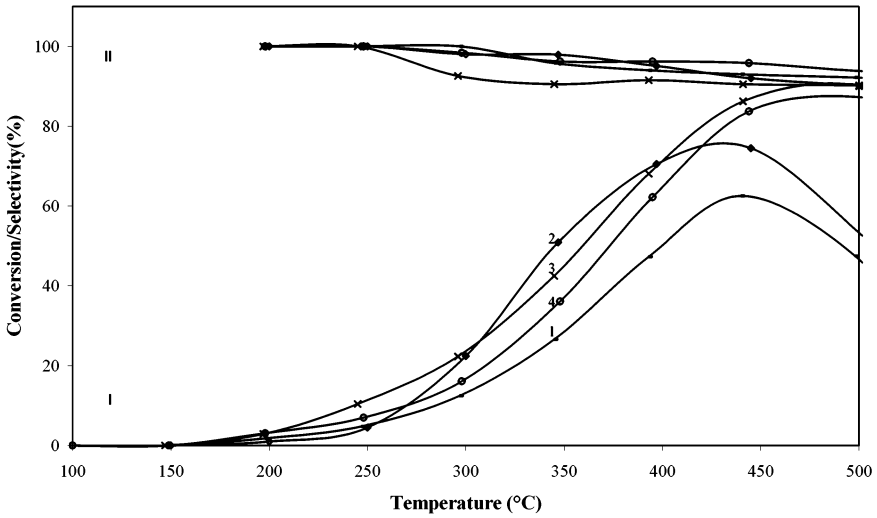

Figure 8. Catalytic activity data of TiO_x/SBA-15 catalysts having (1) 0.17, (2) 0.37, (3) 0.55, and (4) 1.00 mmol of Ti/g in terms of NO conversion (I) and N_2 selectivity (II).

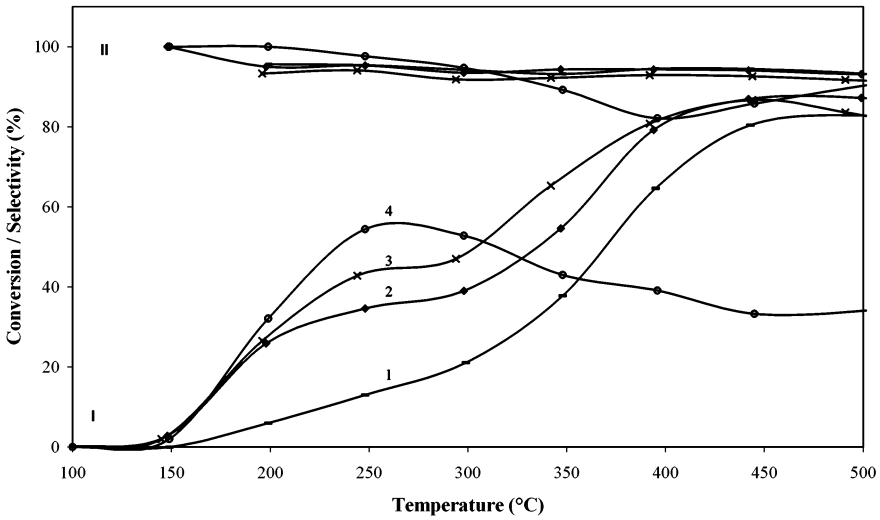

Figure 9. Catalytic activity data of VO_x/SBA-15 catalysts having (1) 0.11, (2) 0.40, (3) 0.45, and (4) 0.77 mmol of V/g in terms of NO conversion (I) and N_2 selectivity (II).

SCR of NO with ammonia over SBA-15 loaded with titanium and vanadium oxide in terms of NO conversion (I) and N_2 selectivity (II) are shown in Figures 8 and 9, respectively.

The catalytic tests were carried out on samples prepared by the MDD method in the liquid phase at RT except for the highest loading of both metals in which the MDD was carried out in the liquid phase at 45 °C. All the catalysts show isolated V and Ti species, as can be seen in the Raman spectra (Figure 7).

The catalytic role of TiO_x is shown in Figure 8. The conversions increase with an increase of Ti loading, to reach their maximum activity at about 430 °C with a NO conversion of ∼85% for the highest Ti content. For the catalysts with the lowest transition metal loadings (samples 1 and 2), the NO conversion increases up to about 430 °C and at higher temperature decreases due to the oxidation of ammonia by oxygen present in the reaction mixture. Samples with a high Ti loading show this decrease at high temperatures. It could be concluded that the surface concentration of titania species determines the ratio of the ammonia conversion in the $DeNO_x$ and NH_3 oxidation processes. The N_2 selectivity is quite high in the whole temperature range studied.

VO_x/SBA-15 catalysts with different V loadings are presented in Figure 9. There is an increase in NO conversion with increasing V loading on the SBA-15. As in the case of the Ti-containing catalyst, the maximum activity is reached at about 430 °C with an ∼85% NO conversion. However, the V-containing catalysts are active within a broader temperature window. For the highest V-content sample, there is a clear decrease at high temperatures most likely caused by the oxidation of ammonia by oxygen. Its N_2 selectivity also slightly decreases, although it remains high. There is no strict correlation between V content and the catalytic activity for SCR in this high temperature region. Probably, textural parameters, loading, and metal dispersion influence the activity of these catalysts at high temperatures. In contrast to the Ti-containing catalysts, the V-containing samples are also active in the low temperature range for the SCR (T < 300 °C). At these temperatures, their catalytic activity increases with increasing V loading. In the low temperature range, ammonia is converted mainly in the $DeNO_x$ process. An increase in the vanadium loading increases NO conversion probably due to the formation of a larger amount of surface VO_x species, which play a role of active sites in this process. At higher temperatures, such vanadia species are active in the ammonia oxidation process. Thus, the highest decrease in NO conversion was measured for the sample with the highest V content.

4. Conclusions

The preparation of SBA-15 supported vanadium and titanium oxide catalysts by the molecular designed dispersion of $VO(acac)_2$ and $TiO(acac)_2$, respectively, has been studied and compared. The bonding mechanisms, the influence of the two metals, and the differences in material properties based on different deposition procedures have been fully investigated. Gas phase deposition leads to a higher vanadium oxide loading on the surface of the SBA-15 compared to the liquid phase procedure. In the latter deposition, high temperatures allow a higher metal oxide loading to be deposited on the support with respect to the room temperature deposition.

After thermolysis in air, supported VO_x and TiO_x on SBA-15 are obtained. Raman spectroscopy measurements reveal that catalysts containing a high metal loading can be prepared with all V species in a strictly tetrahedral configuration and isolated Ti species, without the presence of anatase phase. For both metal oxide catalysts, the MDD method allows the preparation of the samples without the formation of V_2O_5 and TiO_2 clusters, obtaining highly dispersed oxides on the silica support.

Several techniques enable us to elucidate the reaction mechanism. The adsorption of $VO(acac)_2$ under gas phase conditions occurs by a ligand exchange mechanism (*R* value around 1), with the formation of a covalent metal−oxygen support bonding and the loss of a ligand as acetylacetone (Hacac). However, as the treatment temperature decreases, the reaction mechanism shows a combination of the two mechanisms. The adsorption of $TiO(acac)_2$ and $VO(acac)_2$ on the SBA-15 under liquid phase conditions proceeds by hydrogen bonding, as the *R* values for both metal complexes are around 2. For $VO(acac)_2$ however, the maximum surface loading under liquid phase conditions is lower than that in the case of titanium. Ti is more reactive than V toward the surface of the SBA-15. Transmission IR shows also the higher thermal stability of $TiO(acac)_2$ compared to $VO(acac)_2$. According to the BET, XRD, and FT-IR data of the supported vanadium and titanium oxide catalysts, the unique structural properties of the SBA-15 are maintained.

TiO_x/SBA-15 and VO_x/SBA-15 catalysts were also catalytically tested for the SCR of NO with ammonia. Both types of catalysts show about 85% NO conversion at around 400 °C. Moreover, the VO_x/SBA-15 catalysts also show catalytic activity in the low temperature range ($T < 300$ °C). The sample with a high V loading is found to be active at low temperatures, while the catalysts with a lower V content exhibit high activity at higher temperatures.

Acknowledgment. P.C. acknowledges the FWO-Flanders (Fund for Scientific Research-Flanders) for financial support.

References and Notes

(1) Abe, T.; Tachibana, Y.; Iwamoto, M. *Chem. Commun.* **1995**, 1617.
(2) Kataoka, T.; Dumesic, J. A. *J. Catal.* **1988**, *112*, 66−79.
(3) Lemonidou, A. A., Nalbandian, L.; Vasalos, I. A. *Catal. Today* **2000**, *61*, 333−341.
(4) Baltes M.; Collart O.; Van der Voort P.; Vansant E. F. *Langmuir* **1999**, *15*, 5841−5845.
(5) Cool, P.; Van der Voort, P.; Vansant, E. F. In *Encyclopedia of Surface and Colloid Science*; Hubbard, A., Ed.; Marcel Dekker Inc.: New York, 2002; pp 5244−5256.
(6) Baltes, M.; Van Der Voort, P.; Collart, O.; Vansant, E. F. *J. Porous Mater*. **1998**, *5*, 317−324.
(7) Kevin, J. C.; White, M. G. *Langmuir* **1991**, *7*, 1198.
(8) Miller, J. M.; Lakshmi, L. J. *Appl. Catal., A* **2000**, *190*, 197−206.
(9) Hakuli, A.; Kytokivi, A. *Phys. Chem. Chem. Phys.* **1999**, *1*, 1607−1613,
(10) Mitchell, M. B.; Chakravarthy, V. R.; White, M. G. *Langmuir* **1994**, *10*, 4523−4529.
(11) Weckhuysen, B. M.; Keller, D. E. *Catal. Today* **2003**, *78*, 25−46.
(12) Gao, X.; Wachs, I. E. *Catal. Today* **1999**, *51*, 233−254.
(13) Hoang-Van, C.; Zegaoui, O.; Pichat, P. *J. Non-Cryst. Solids* **1998**, *225*, 157−162.
(14) Blanco, J.; Avila, P.; Suarez, S.; Martin, J. A.; Knapp, C. *Appl. Catal., B* **2000**, *28*, 235−244.
(15) Bond, G. C.; Tahir, S. F. *Appl. Catal.* **1991**, *71*, 1−31.
(16) Wachs, I. E.; Saleh, R. Y.; Chan, S. S.; Chersic, C. *CHEMTECH* **1985**, *15*, 756.
(17) Lakshmi, J. L.; Ihasz, N. J.; Miller, J. M. *J. Mol. Catal. A: Chem.* **2001**, *165*, 199−209.
(18) Berndt, H.; Martin, A.; Bruckner, A.; Schreier, E.; Muller, D.; Kosslick, H.; Wolf, G.-U.; Lucke, B. *J. Catal.* **2000**, *191*, 384−400.
(19) Fornes, V.; Lopez, C.; Lopez, H. H.; Martinez, A. *Appl. Catal., A* **2003**, *249*, 345−354.
(20) Baltes, M.; Van Der Voort, P.; Weckhuysen, B. M.; Rao, R. R.; Catana, G.; Schoonheydt, R. A.; Vansant, E. F. *Phys. Chem. Chem. Phys.* **2000**, *2*, 2673−2680.
(21) Van Der Voort, P.; Baltes, M.; Vansant, E. F. *J. Phys. Chem. B* **1999**, *103*, 10102−10108.
(22) Schrijnemakers, K.; Vansant, E. F. *J. Porous Mater*. **2001**, *8*, 83−90.
(23) Van Der Voort, P.; Van Welzenis, R.; De Ridder, M.; Brongersma, H. H.; Baltes, M.; Mathieu, M.; Van de Ven, P. C.; Vansant, E. F. *Langmuir* **2002**, *18*, 4420−4425.
(24) Zhao, D.; Huo, Q.; Feng, J.; Chmelka, B. F.; Stucky, G. D. *J. Am. Chem. Soc.* **1998**, *120*, 6024−6036.
(25) Vogel, A. I. *Quantitative Inorganic Analysis*, 3rd ed.; Longman: London, 1971; p 790.
(26) Van Der Voort, P.; Possemiers, K.; Vansant, E. F. *J. Chem. Soc., Faraday Trans.* **1996**, *92*, 843−848.
(27) Van Der Voort, P.; White, M. G.; Mitchell, M. B.; Verberckmoes, A. A.; Vansant, E. F. *Spectrochim. Acta, Part A* **1997**, *53*, 2181−2187.
(28) De Boer, J. H.; Linsen, B. G.; Osinga, T. *J. Catal.* **1964**, *4*, 643.
(29) Meynen, V.; Segura, Y.; Cool, P.; Vansant, E. F. *Microporous Mesoporous Mater.*, in press.
(30) Segura, Y.; Cool, P.; Van Der Voort, P.; Mees, F.; Meynen, V.; Vansant, E. F. *J. Phys. Chem. B* **2004**, *108*, 3794−3800.